Core–Shell Metal Zeolite Composite Catalysts for In Situ Processing of Fischer–Tropsch Hydrocarbons to Gasoline Type Fuels

Jan Přech, Debora R Strossi Pedrolo, Nilson R Marcilio, Bang Gu, Aleksandra S Peregudova, Michal Mazur, Vitaly Ordomsky, Valentin Valtchev, Andrei y Khodakov

Revision, January 22nd, 2020

Core-Shell Metal Zeolite Composite Catalysts for *In Situ* Processing of Fischer-Tropsch Hydrocarbons to Gasoline Type Fuels

Jan Přech[a], Debora R. Strossi Pedrolo[b, c], Nilson R. Marcilio[c], Bang Gu[b], Aleksandra S. Peregudova[b], Michal Mazur[d], Vitaly V. Ordomsky[b], Valentin Valtchev[a] and Andrei Y. Khodakov[b]*

[a]*Laboratoire Catalyse et Spectrochimie, ENSICAEN, 6 Boulevard Maréchal Juin 14050 Caen, France*

[b]*Univ. Lille, CNRS, Centrale Lille, ENSCL, Univ. Artois, UMR 8181 – UCCS – Unité de Catalyse et Chimie du Solide, F-59000 Lille, France*

[c]*Departamento de Engenharia Química, Universidade Federal do Rio Grande do Sul - UFRGS, Porto Alegre, RS 90040-040, Brazil*

[d]*EaStCHEM School of Chemistry, University of St Andrews, St Andrews, KY16 9ST, UK*

[*]Corresponding author: andrei.khodakov@univ-lille.fr

Abstract

Fischer-Tropsch synthesis has two main challenges related to direct production of gasoline fuels. First, the chain length distribution of the products follows a broad and unselective Anderson-Schulz–Flory distribution. Second, mostly linear hydrocarbons are formed in the Fischer-Tropsch reaction, thus requiring isomerization while manufacturing gasoline fuels. The present paper addresses a synthetic strategy for the preparation of hierarchical metal and zeolite nanocomposite catalysts for direct synthesis of iso-paraffins from syngas. The nanocomposites are synthesized in three steps. In the first step, the parent (core) zeolite is etched with an ammonium fluoride solution. The etching creates small mesopores inside the zeolite crystals. In the second step, the Ru nanoparticles prepared using water-in-oil microemulsion are deposed in the mesopores of the zeolite. In the third step, a zeolite shell of MFI-type zeolites (silicalite-1 or ZSM-5) is grown on the parent zeolite crystals coating both the etched surface and metallic nanoparticles. Thus, the metal nanoparticles become entirely encapsulated inside the zeolite matrix.

Most important parameters such as ruthenium content, zeolite mesoporosity and more particularly the acidity of the catalyst shell, which affect the catalytic performance of the synthesized nanocomposite materials in low temperature Fischer-Tropsch synthesis were identified in this work. The higher relative amount of iso-paraffins was observed on the catalysts containing a shell of ZSM-5. The proximity between metal and acid sites in the zeolite shell of the nanocomposite catalysts is a crucial parameter for the design of efficient metal zeolite bifunctional catalysts for selective synthesis of gasoline type fuels via Fischer-Tropsch synthesis, while the acidity of the catalyst core has only a limited impact on the catalytic performance.

Keywords: hierarchical zeolite; core-shell structure; nanocomposite; ruthenium; Fischer-Tropsch synthesis; bifunctional catalyst; isomerization

1. Introduction

The second-generation biofuels (gasoline, diesel, etc.) use all types of non-edible biomass, such as lignocellulosic biomass, organic residues, wastes. The Biomass-to-Liquid (BTL) thermochemical technology is based on the destruction of biomass by gasification and formation of syngas. Syngas might be further converted into paraffins, olefins and alcohols by Fischer–Tropsch (FT) synthesis. In the FT synthesis, the catalyst active phase is usually made of VIII group transition metals; the choice of the active phase depends on various factors such as the target product (fuels or chemicals), operating conditions and cost[1, 2].

The traditional FT technologies have two main challenges related to the direct production of gasoline. First, the chain length distribution of the products follows the statistical Anderson-Schulz–Flory distribution (ASF), which implies the same chain growth probability (α) for all hydrocarbons. Therefore a specific range of the hydrocarbons cannot be produced with a significant yield. The yield of the C_5-C_9 hydrocarbons (gasoline fraction) is limited to less than 50 % by the ASF polymerization statistics. Second, mostly linear hydrocarbons are formed and thus, an isomerization of the crude FT hydrocarbons is required for production of high-octane gasoline fuels [3].

Since the temperature for low temperature FT synthesis and isomerization are rather similar, syngas can be also converted to iso-pararafins in a single process over bifunctional catalysts. The selectivity to the branched hydrocarbons in direct syngas conversion can be improved by adding

an acid function to the FT catalysts [4,5]. The acidic function is usually provided by a zeolite, such as ZSM-5, beta and mordenite. In the bifunctional catalysts, the concentrations, intrinsic activities of the metal and acid sites and in particular, their localization within the catalyst, are extremely important for the catalytic performance [6]. The close proximity, "site intimacy", between the metal and acid sites is required to attain maximum activity and selectivity in many reactions of bifunctional catalysis.

Several configurations of metallic and acid functions in the bifunctional catalysts and combining FT-isomerization process have been described in the literature [7–11]. Dual-bed reactors with an acidic zeolite downstream from a conventional FT catalyst and hybrid catalysts containing a physical mixture of the two components have mainly been utilized for the production of gasoline-range (C_5-C_{12}) hydrocarbons. However, the isomerization efficiency of these catalytic systems has been insufficient. Indeed, the transformation of the formed wax by hydrocracking over metal-free zeolites requires higher temperatures. The yield of gasoline products remains low ($C_{iso}/C_n<0.2$) because of poor contact between the formed wax and acid sites in the zeolites. Addition of a metal to the zeolite, usually via impregnation or ion-exchange, is often the first step in the preparation of the composite catalyst [12] . However, metal ions partially participate in the ion exchange with the acid sites and thus, neutralize the acidic function. In addition, significant diffusion limitations because of extremely small pore sizes of zeolites (typically 0.5-0.7 nm) lead to slow diffusion of hydrocarbons inside the micropores of the zeolite. The use of mesoporous (hierarchical) zeolites for synthesis of bifunctional catalysts is a common approach to overcome the diffusional limitations and to increase carbon monoxide conversion [13].

Localization of metal nanoparticles inside the zeolite micropores also introduces shape-selectivity effects for the formed hydrocarbons [14,15]. Recently, we found [16] that FT reaction

selectivity to short chain iso-paraffins was principally affected by the zeolite acidity, while the selectivity to slowly diffusing long-chain hydrocarbons mostly depended on the proximity between the metal and acid sites. The use of cobalt-zeolite nanocomposites with cobalt nanoparticles selectively located inside the zeolite pores led to significantly higher selectivity to the C_5-C_{12} branched hydrocarbons in FT synthesis [17]. However, the stability of the composite catalysts prepared by impregnation is a critical issue. In the presence of reaction mixture and in particular water, metal nanoparticles can migrate out the zeolite pores and agglomerate on the zeolite outer surface. This results in formation of large metal nanoparticles on the zeolite surface and decrease in both reaction rate and selectivity to iso-paraffins. In addition, diffusion limitations result in higher selectivity to methane, which is a low cost product, and thus decreases the yield of the desired longer hydrocarbons [18]. To increase efficiency of the secondary (isomerization) reactions in the bifunctional process, Tsubaki and co-workers [19,20] and Zhu and Bollas [21] designed capsule core–shell catalytic systems, which contain conventional FT catalyst such as Co/SiO_2 or Co/Al_2O_3 in the core and an acidic zeolite membrane shell on the surface of the catalyst grains.

Another approach involves using Co/SiO_2 as precursor of Co-zeolite catalysts [22–24]. In principle, the SiO_2 carrier acts as a silica source for the zeolite (ZSM-5) crystallization, while the Co_3O_4 nanoparticles become encapsulated in the formed zeolite. The developed bifunctional catalysts exhibit high selectivity to gasoline range of hydrocarbons with a higher yield of isomers in comparison with hybrid and composite catalysts prepared by impregnation. Nevertheless, a thin layer of the zeolite on the surface of metallic catalyst cannot provide high efficiency in isomerization of the produced hydrocarbons. Increase in the zeolite layer thickness increases diffusion limitations and thus methane production. Metal species can also be added directly into

a conventional zeolite synthesis gel [25], but they often result in uncontrollable metal distribution within the zeolite crystals. Recently, we proposed [27, 28] introduction of metal species to the zeolites during their synthesis using metal containing carbon nanotubes as secondary hard templates. The metal carbon nanotube templates play several roles [27]; first they serve as a replica to create zeolites with specific fibrous morphology. Second, they markedly increase the zeolite secondary porosity. Finally, metal carbon nanotube templates introduce the metal nanoparticles uniformly inside the mesoporous zeolites, however, without their complete encapsulation.

In this manuscript, we propose a new strategy for the synthesis of efficient metal zeolite bifunctional catalysts for the direct synthesis of branched gasoline type hydrocarbons from syngas. This strategy addresses nanocasting of preformed ruthenium metallic nanoparticles in a secondary pore system of a mesoporous zeolite. The metal nanoparticles located in the mesopores of the zeolite are then entirely encapsulated by secondary grown zeolite structure. This new approach offers a number of advantages. First, the separate preparation of metal nanoparticles allows a fine control of their sizes, morphology and chemical composition. In contrast to the in-situ synthesis of metal nanoparticles inside of the zeolites pores, the impact of the zeolite matrix on the size and shape of the nanoparticles is suppressed. Futhermore, the nanoparticles are stabilized in the encapsulated systems thus suppressing the particle migration and sintering. Finally, the proximity between metal and zeolite active sites provides an unravelled synergy between the two types of the sites in the catalyst**.** The zeolite performance in hydrocarbon isomerization is mostly affected by the composition of the zeolite shell. The prepared catalysts were characterized using a wide range of techniques, which provide information on their morphology, structure, texture and chemical composition. Their catalytic

performance in the FT reaction was evaluated under high pressure in a fixed bed microreactors using a high throughput catalytic setup.

2. Experimental

2.1.Synthesis of parent zeolites used as cores

Two different parent zeolites have been used for the preparation of the metal zeolite composite catalysts. A sample of ZSM-5 zeolite (**MFI** structure) with Si/Al=21 was obtained from Süd-Chemie in the NH_4^+ form. The ZSM-5 has uniform coffin shaped crystals, size about 4x2x1 µm. Silicalite-1 (S-1, purely siliceous **MFI** zeolite) was synthesised as follows: 114 ml of 1 M solution of tetrapropylammonium hydroxide (TPA-OH, Alfa Aesar) were diluted with 97.8 g of distilled water and subsequently 65.1 g of Ludox HS-30 colloidal silica (30 wt.% of SiO_2, Sigma Aldrich) was added dropwise under vigorous stirring. The synthesis mixture with a molar composition 100 SiO_2 : 35 TPA-OH : 4000 H_2O was homogenized for 1 h at room temperature and subsequently transferred in a 0.5 l Teflon-lined autoclave with a magnetic stirrer. The hydrothermal synthesis occurred at 175°C, with the stirring rate of 300 rpm, for 25 h. The solid product was filtered, washed with copious amount of water, dried at ambient temperature and finally calcined in static air at 500°C for 10 h with a temperature ramp of 1°C/min. The sample has morphology of irregular crystals having 3-5 µm in size.

2.2.Zeolite etching

The etching of the parent zeolites follows the procedure described in Ref. [28]. A 40 wt.% solution of NH_4F was prepared from 80.0 g of NH_4F (98%, Sigma-Aldrich) and 120.0 g of distilled water. The solution was pre-heated to 50°C (+/- 2°C) in the 40 kHz ultrasonic bath in an open vessel

equipped with a mechanical stirrer. Then, 10 g of the parent zeolite were introduced into the solution under stirring and ultrasound radiation. The etching occurred for 30 min (ZSM-5) or 13 min (S-1) under the above conditions. After the given time, the suspension was quickly filtered on a Buchner funnel and washed several times with distilled water (about 500 ml all together). The solid product was dried at 90°C and characterized. Note that NH_4F solution is a contact poison; use appropriate safety devices.

Before any further use, the etched ZSM-5 was ion-exchanged into Na^+ form; using 1M solution of $NaNO_3$ for 4 h at room temperature. The procedure was repeated 4 times as 100 ml of solution per 1 g of zeolite was used. After the treatment, the zeolite was filtered, washed twice with 100 ml/g of water and dried at ambient temperature. The etched S-1 was used without any further pre-treatment. Please note that the Ru/ZSM-5 and Ru/S-1 labels correspond to the etched zeolites.When the zeolite was non-etched , this is specified explicitly.

2.3.Preparation of Ru nanoparticles and their insertion in zeolite

Ruthenium nanoparticles were prepared following the procedure from Ref.29. Initially, two micro-emulsions were prepared. Micro-emulsion I was prepared from 3.00 g of hexadecyltrimethylammonium bromide (CTABr, 96%, Sigma-Aldrich), 5.00 g of 1-hexanol (98%, Sigma-Aldrich) and 2 g of 0.5 M aqueous solution of $RuCl_3$ (Ru content 45-55%, Sigma-Aldrich). Micro-emulsion II was composed of 3.00 g of CTABr, 5.00 g of 1-hexanol and 2 g of 1.5 M aqueous solution of $NaBH_4$ (96%, Sigma-Aldrich). Both micro-emulsions were homogenized for 30 min and subsequently emulsion II was added dropwise into emulsion I under vigorous stirring (750 rpm). The combined emulsions were stirred for another 30 min to finish the reduction and then 500 mg of the etched zeolite (Na^+ form in the case of ZSM-5) was

added and stirring continued for another 2 h. After this time, the emulsion was diluted with about 20 ml of ethanol (96%) filtered and the solid black product was washed with ethanol and subsequently with water (about 200 ml of each). Finally, the product was dried at ambient temperature and subjected to the overgrowing or calcined in static air at 480°C for 5 h with temperature ramp 2°C/min. The Ru nanoparticles deposition on parent zeolites was performed using the same procedure. The sample was calcined after the nanoparticle deposition.

2.4.Coating the Ru-zeolite catalysts with S-1 shell

For the preparation of S-1 shell, a coating solution with a molar composition of 12 TPA-OH : 100 SiO_2 : 5800 H_2O was prepared from 1M TPA-OH solution, tetraethyl orthosilicate (98%, Sigma-Aldrich) and distilled water. After mixing all the three components, the mixture was stirred overnight to obtain a clear homogenous solution.

This solution was combined with the non-calcined product of the insertion step (see section 2.3) using 25 g of solution/1 g of the material after insertion. The overgrowing solution and etched zeolite were stirred together for 2 h and then subjected to the secondary zeolite crystallization in a tumbling Teflon-lined autoclave (50 rpm) at 150°C for 15 h. After the given time, the crude product was filtered, washed with distilled water, dried at ambient temperature and calcined in static air starting at 110°C for 2 h and then at 480°C for 5 h with a temperature ramp 2°C/min.

2.5.Coating the Ru-zeolite catalysts with the ZSM-5 shell

The ZSM-5 shell was crystallized from a coating solution with a molar composition of 25 TPA-OH : 100 SiO_2 : 3.33 $Al(OH)_3$: 5800 H_2O (Si/Al=30). It was prepared from 1M TPA-OH solution, tetraethyl orthosilicate (98%, Sigma-Aldrich), aluminum hydroxide (Aldrich) and

distilled water. After mixing all four components, the solution was stirred overnight to obtain clear homogenous solution. The coating procedure was the same as described above for S-1 shell with the exception that crystallization of the shell occurred at 140°C for 4 h. After workup of the coating mixtures, the samples were calcined in static air starting at 110°C for 2 h and then at 480°C for 5 h with a temperature ramp 2°C/min.

2.6.Ion exchange and reduction

The calcined samples were ion-exchanged into the NH_4^+ form by four-stage treatment with 1 M NH_4NO_3 solution (100 ml/g of zeolite, 4 h each time). Finally, the samples were converted into H^+-form by calcination at 450°C for 2 h (ramp 2°C/min). For characterization, a part of the catalysts was reduced in a flow of hydrogen (100 ml/min) in a slowly rotating oven at 400°C for 5 h (ramp 2°C/min). The samples, which were used in the catalytic tests, were reduced in the reactor just before running the catalytic test.

2.7.Characterization techniques

The X-ray powder diffraction patterns (XRD) were measured with a PANanalytical X'Pert PRO diffractometer using CuKα radiation (λ = 0.15418 nm). The data were collected in continuous mode over the 2θ range of 5-50° using a ¼° divergence slit. Scanning electron microscopy (SEM) images were collected on a MIRA TESCAN microscope equipped with a field emission gun. The images were collected with an acceleration voltage of 30 kV.

The high-resolution transmission electron microscopy (HRTEM) was performed two different machines. The first one was Jeol JEM-2011 microscope operating at the accelerating voltage of 200 kV. The HRTEM images were recorded with a Gatan 794 CCD camera. The camera length,

sample position, and magnification were calibrated using standard gold film methods. A part of the images was collected also using a Tecnai instrument, equipped with a LaB_6 crystal, operating at 200 kV. Prior to the analysis, the samples were dispersed by ultrasound in ethanol solution for 5 min, and a drop of solution was deposited onto a carbon membrane onto a 300 mesh-copper grid.

Nitrogen adsorption/desorption isotherms were measured at liquid nitrogen temperature (-196°C) using a Micromeritics Triflex instrument. Before the measurements, the samples were degassed under vacuum of turbomolecular pump at 300°C for 6 h. The BET area was evaluated using adsorption data in the range of a relative pressure from $p/p_0 = 1.1. 10^{-7}$ to $p/p_0 = 0.01$ (corresponding to the growing part of Rouquerol BET plot). The t-plot method [30] was applied to determine the external surface area (S_{ext}). Micropore volume (V_{mic}) was determined from BJH pore size analysis using a model for N_2 on oxide surface with cylindrical geometry (part of the Micromeritics user software). Adsorbed amount of nitrogen at $p/p_0 = 0.95$ was used to determine total pore volume (V_{total}).

The Si/Al ratio of the samples was determined by an ICP-OES analysis. The samples were dissolved in a mixture of HF and Aqua Regia before the analysis. Ruthenium content was determined from hydrogen consumption in Temperature-programmed Reduction (TPR). The TPR experiments were performed using a Micromeritics Autochem II 2920 instrument. Before the analysis, ruthenium was turned into RuO_2 by calcination in air at 500 °C for 3 h. The TPR was conducted in the range from 100 to 1000°C with a temperature ramp of 10°C/min. A typical RuO_2 reduction temperature was 180°C.

The concentration of acid sited was determined from pyridine titration using IR spectroscopy. The individual samples were diluted 3 times with silica (Aldrich) to maintain sufficient

transparency, pressed into self-supporting wafers with a density of 8.0–12 mg/cm^2 and activated at 450°C for 5 h with a temperature ramp 2°C/min under vacuum of turbomolecular pump (final pressure 1.0-1.5 10^{-6} torr). The amount of acid sites was determined from adsorption/desorption of pyridine (Py) at 150°C. Adsorption occurred for 30 min at partial pressure 1 torr, followed by desorption at 150°C for 15 min under vacuum of turbomolecular pump. This time is sufficient to stabilize amount of adsorbed pyridine. The spectra were collected with a Thermo Scientific Nicolet 6700 FT-IR spectrometer at 4 cm^{-1} optical resolution by collecting 128 scans for a single spectrum. The spectra intensities were recalculated to a wafer density of 10 mg/cm^2. The concentrations of acid sites were determined from integral intensities of bands at 1454 cm^{-1} (Lewis) and at 1545cm^{-1} (Brønsted acid sites) using extinction coefficients, ε(L) = 1.28 cm/μmol, and ε(B) =1.13 cm/μmol [31].

2.8.Catalytic testing

Carbon monoxide hydrogenation (Fisher-Tropsch reaction) was carried out on REALCAT platform in a Flowrence® high-throughput unit (Avantium) equipped with 16 parallel milli-fixed-bed reactors (d=2 mm) operating at the pressure of 20 bar, H_2/CO= 2 molar ratio, T=220 ºC and GHSV from 4.8 -6.5 L h^{-1} g_{cat}^{-1}. The catalyst loading was 50 mg per reactor. Prior to the catalytic test, all the samples were activated in a flow of hydrogen at atmospheric pressure during 10 h at 400 °C. During the activation step, the temperature ramp was 3 °C/min. After the reduction, the catalysts were cooled down to 180 °C and a flow of premixed syngas was gradually introduced to the catalysts. When the reactor attained required pressure, the temperature was slowly increased to the temperature of the reaction. The reaction has been conducted for 60 h at different GHSV of syngas. Gaseous reaction products were analyzed by

on-line gas chromatography. The analysis of permanent gases was performed using a Molecular Sieve column and a thermal conductivity detector. The C_1-C_4 hydrocarbons were separated in a PPQ column and analyzed by a thermoconductivity detector. The C_5-C_{12} hydrocarbons were analyzed using a CP-Sil5 column and a flame-ionization detector. The carbon monoxide contained 5 % of helium, which was used as an internal standard for calculating carbon monoxide conversion. The product selectivity (S) was reported as the percentage of CO converted into a given product and expressed on carbon basis.

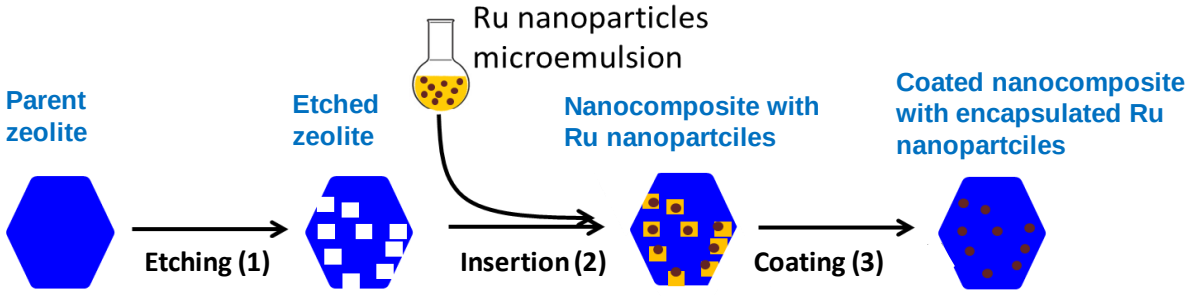

Scheme 1: Synthesis of the zeolite catalysts with encapsulated ruthenium nanoparticles**.**

3. Results and discussion

3.1.Strategy for the synthesis of zeolite catalysts with encapsulated metal nanoparticles

The synthesis of the metal-zeolite composite catalysis with encapsulated metal nanoparticles is composed of 3 major steps (**Scheme 1**). In the first step (etching), the parent (core) zeolite is treated with a 40% NH_4F solution [28]. The etching creates small mesopores inside the zeolite crystals and sort of cups on the surface of the crystals, which accommodate metallic nanoparticles in the second step (insertion) and serves as nucleation sites in the third step (coating). The Ru nanoparticles were prepared using water-in-oil microemulsion following the procedure [29] and then deposed in the mesopores of the zeolite. Ruthenium nanoparticles are

introduced in the second step (insertion) into the etched zeolite. In the third step (coating), the zeolite shell crystallizes on the surface of parent crystals covering both etched surface and metallic nanoparticles, which become trapped inside the zeolite matrix. The resulting composite samples are denoted as shell/metal/core (e.g. ZSM-5/Ru/S-1 means the sample has a core (parent) crystal of S-1, ruthenium nanoparticles and it was coated by a ZSM-5 shell).

In the present study, the Ru-zeolite composites with various combination of core and shell materials (either acidic ZSM-5 or inert S-1) were prepared. In addition, the non-coated composites Ru/ZSM-5, Ru/S-1, Ru/non-etched-ZSM-5 and Ru/non-etched-S-1 have been also tested.

3.2.Catalyst structure

The prepared catalysts were characterized by a combination of techniques. **Figure 1** presents the SEM images of the ZSM-5/Ru/ZSM-5 and ZSM-5/Ru/S-1 catalysts at different stages of the synthesis. The parent ZSM-5 zeolite (**Figure 1 A**) has regular coffin-shaped crystals sometimes forming twins with a size of approximately 3-4 μm in the longest dimension. Parent S-1 (**Figure 1 F**) is composed of irregular crystals having 3-5 μm in diameter. Upon the fluoride etching, the crystal twins are separated, leaving regular holes in the crystals and creating characteristic rough surfaces on the planes, where the two crystals were in contact (**Figure 1 B, G**). These rough surfaces are ideal places to accommodate the Ru nanoparticles. They can also act as seeds for the crystallization of the new (coating) zeolite phase in the catalyst shell. After the insertion, some of the nanoparticles agglomerate, while the rest is dispersed on the surface and accommodated in the etched mesopores (cf. TEM image Ru/ZSM-5) - images collected using BSE (back-scattering electron) detector highlights the presence of dense metallic phase (**Figure 1 D,I**). Upon

subsequent crystallization (coating), a thin layer of small ZSM-5 crystals is formed and encapsulates the Ru nanoparticles inside the zeolitic phase (**Figure 1 E, J**). Note that original shape of the parent crystals can be clearly identified by SEM and TEM through all the stages. The S-1 shell crystallizes in slightly different morphology. The formed phase appears better connected to the parent crystals (**Figure 2**) and it has more uniform surface. Moreover, formation of some larger (200-500 nm) secondary S-1 crystals occurred, however their amount was relatively low.

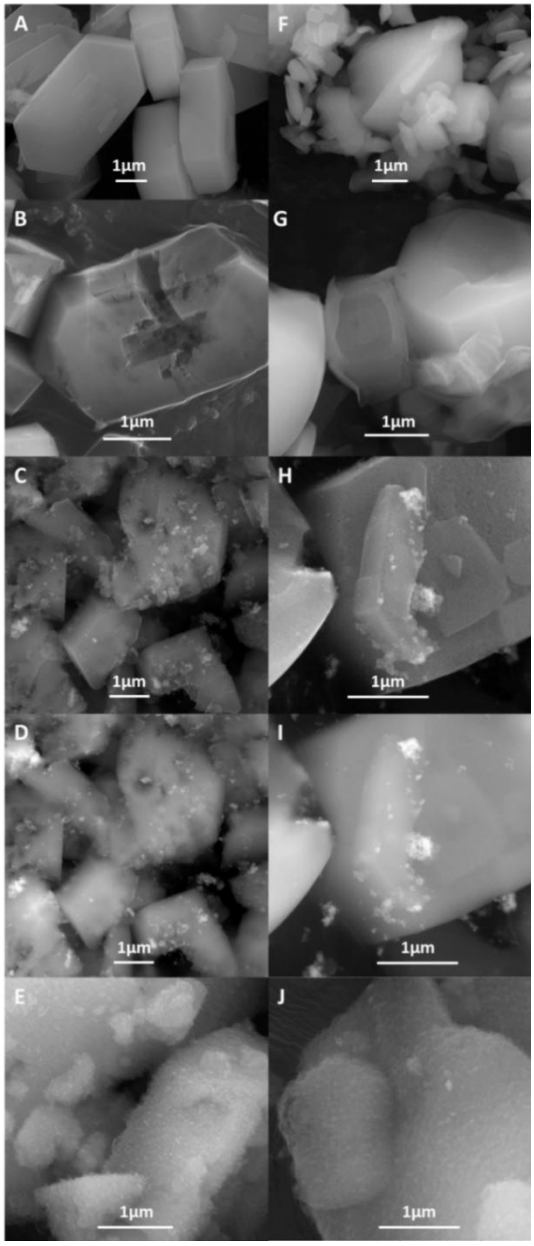

Figure 1: SEM images of the ZSM-5/Ru/ZSM-5 (A-E) and ZSM-5/Ru/S-1 (F-J) in the course of the synthesis: parent ZSM-5 (A), S-1 (F); fluoride etched ZSM-5 (C) and S-1 (G); Ru/ZSM-5 and Ru/S-1 after insertion of Ru nanoparticles and calcination in the view of secondary electron (conventional) detector (C,H) and BSE detector (D,I); final overgrown ZSM-5/Ru/ZSM-5 (E) and ZSM-5/Ru/S-1 (J).

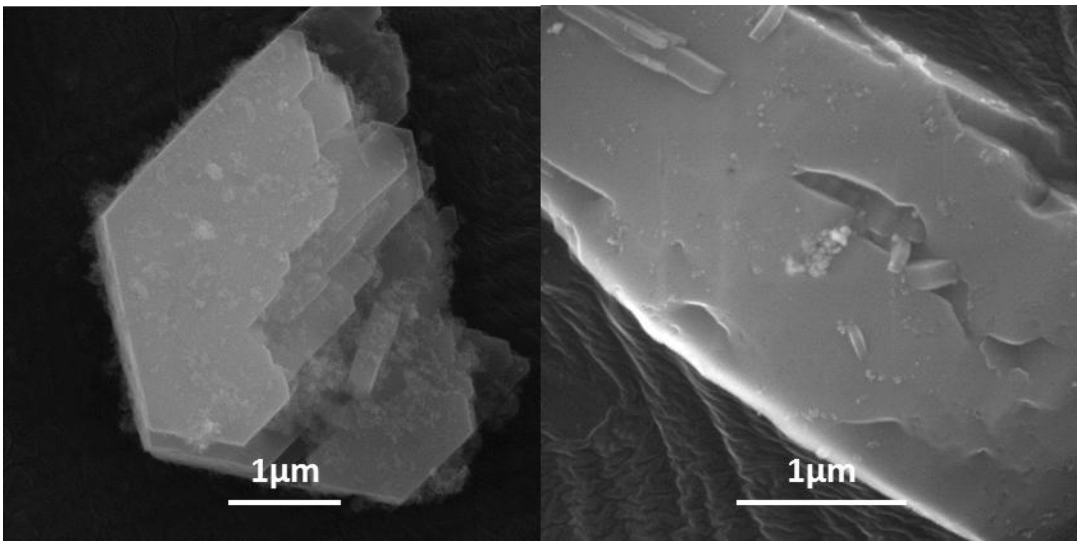

Figure 2: SEM images of ZSM-5/Ru/S-1 (S-126, left) and S-1/Ru/S-1 (S-137, right).

The catalyst synthesis was followed by powder XRD. **Figure 3** shows representative XRD patterns for ZSM-5/Ru/ZSM-5 in the final stages of the synthesis. The patterns for the other catalysts did not differ significantly. After the Ru insertion (data not presented) and coating (**Figure 3**, ZSM-5/Ru/ZSM-5 as-synthesized), the XRD patterns of the as-synthesized catalyst contained only the patterns of **MFI** zeolite. No XRD peaks attributed to the ruthenium phases were observed. This is an indirect proof that the Ru nanoparticles are too small to be detected by XRD. The size of Co nanoparticles prepared by Subramanian [29] et al. using the same method was approximately 5 nm. We expect therefore, the Ru nanoparticles formed in microemulsion to be of a similar size. After calcination, broad reflections of the RuO_2 phase appear in the XRD pattern at (2θ = 28.05° and 35.1°) because the metallic ruthenium quickly oxidize to the oxide, when exposed to oxygen at elevated temperature (during calcination). The appearance of the lines points to the increase in the particle size due to some sintering during the calcination and oxidation of the metal. The RuO_2 particle size in the final catalysts is about 20 nm (see below). Nevertheless, the RuO_2 can be easily reduced back to Ru in hydrogen atmosphere, exhibiting

broad XRD lines at 2θ = 38.5°, 42.3° and 44.2°. The reduction of the catalysts was performed *in-situ* after charging into the reactor. SEM (**Figure 1**) and TEM images (**Figure 4**) suggest that the Ru diffraction lines are mostly relevant to the Ru agglomerates, which can sinter to form larger Ru crystals. XRD patterns of all the discussed catalysts are also presented in **Figures S1** and **S2, Supporting Information (SI).** Note that all the XRD patterns exhibit a straight baseline, which (together with the textural properties analysis, *vide infra*) proves the crystallinity of the coating shell. For comparison, the XRD pattern of a catalyst with amorphous silica shell is shown in **Figure S3, SI**. In this image, a baseline elevation between 2Θ = 15° - 30° can be observed, which is characteristic of amorphous silica.

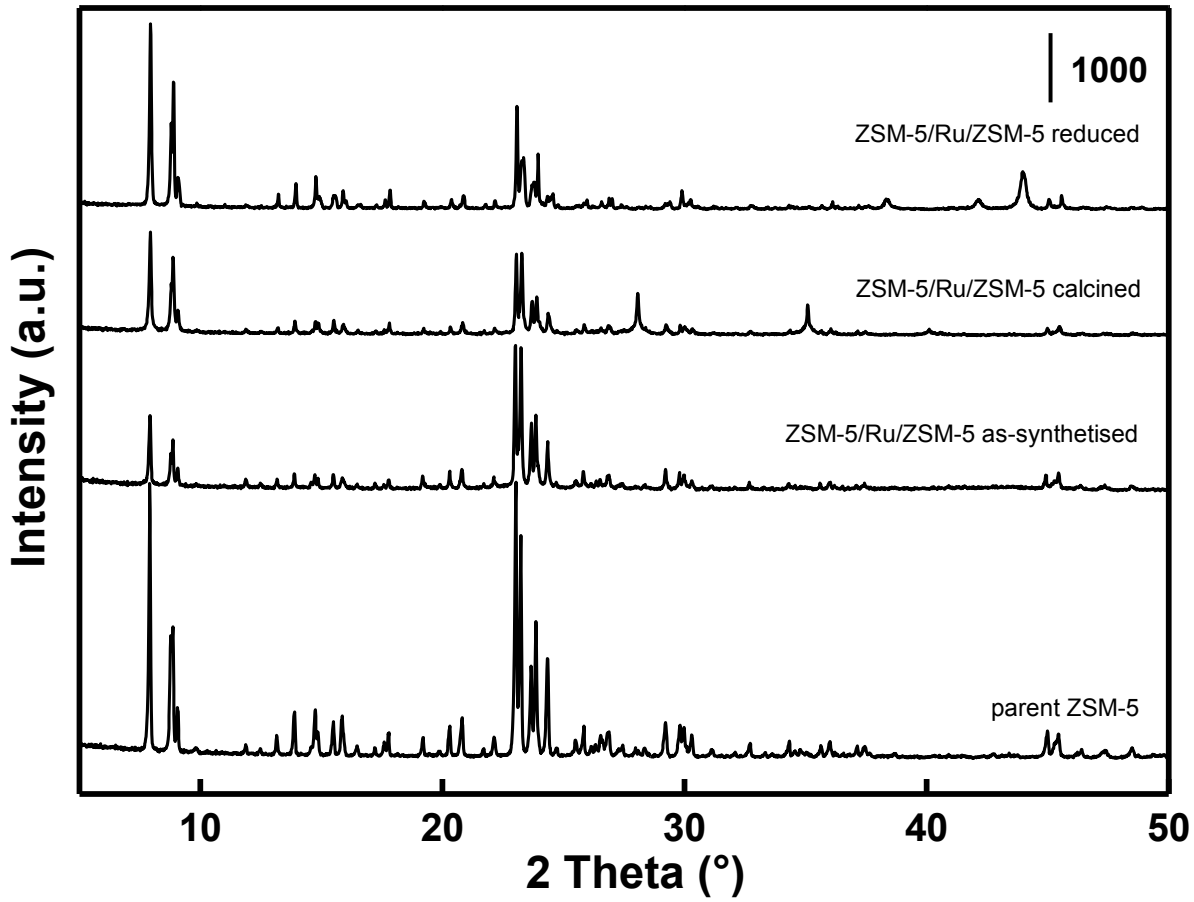

Figure 3: Powder XRD patterns for the ZSM-5/Ru/ZSM-5 at different stages of the synthesis.

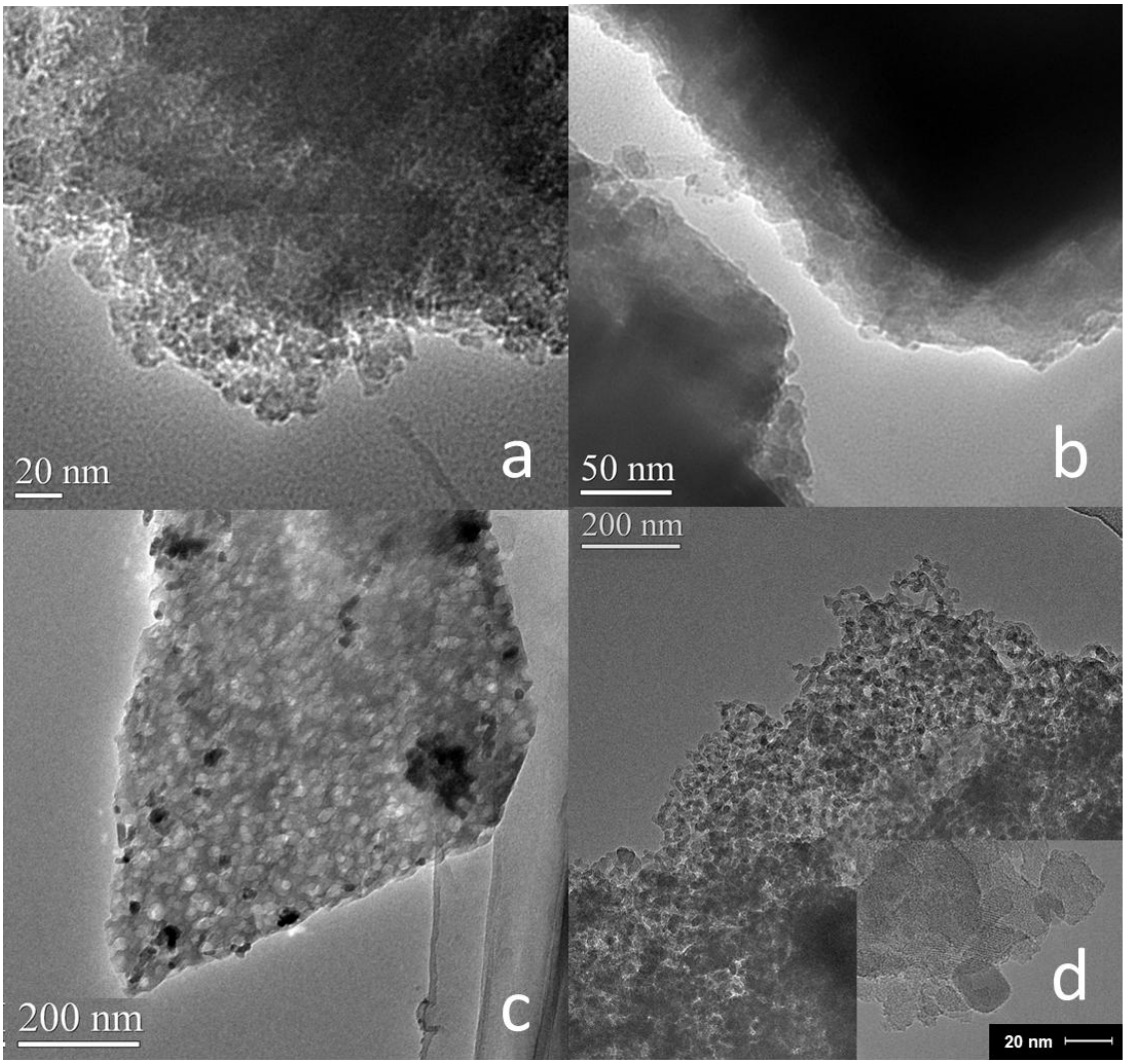

Figure 4: TEM images of the composite catalysts: (a) ZSM-5/Ru/ZSM-5, (b) ZSM-5/Ru/S-1, (c) Ru/ZSM-5, (d) S-1/Ru/ZSM-5.

Figure 4 presents TEM images of the catalysts with a shell on the surface of the parent (core) crystals and a fragment of parent crystal having no shell (Ru/ZSM-5). The TEM image of the Ru/ZSM-5 catalyst, (**Figure 4 c**) shows the presence of small mesopores formed by the fluoride etching. Previously we showed [28] that the mesopores created by fluoride etching might have

rectangular shape. The histogram of particle size distribution has (**Figure S4, SI**) shown that in Ru/ZSM-5 mostly contains the particles smaller than 25 nm. It also reveals Ru nanoparticles in these small mesopores where, in some cases; they adopt their size and shape. In the images of the coated catalysts, particularly these with the ZSM-5 shell (**Figure 4 a,d**), the nanoparticles are covered with the small ZSM-5 crystals formed during the coating. The insert in **Figure 4 d** illustrates typical Ru nanoparticles (darker round spots in middle bottom of the image) size of about 10-20 nm but even smaller nanoparticles can be found e.g. in **Figure 4 a**. Thus, we conclude the size of Ru nanoparticles inside the zeolite crystals ranges between about 3 and 20 nm. The TEM image of S-1/Ru/ZSM-5 (**Figure 4 b**) confirms that the S-1 shell is more uniform in comparison with the ZSM-5 overgrown catalysts and as a result, the nanoparticles are more difficult to be observed.

The characterization data are summarized in **Table 1**. In general, all the catalysts exhibit similar textural properties, since their structure is essentially the same. S-1/Ru/ZSM-5 and S-1/Ru/S-1 (the two with S-1 shell) have slightly lower BET surface area and micropore volume in comparison with their ZSM-5 shell analogues (e.g. BET = 320 m^2/g *vs.* 400 m^2/g and 346 m^2/g vs. 404 m^2/g, respectively). This probably points to a lower crystallinity of the S-1 shell in comparison with ZSM-5. The Ru content varies between 6 and 8.4 wt.% for all the catalysts, except for the pair Ru/S-1 and Ru/ZSM-5 (11.2 wt.% and 10.9 wt.%, respectively), because these two catalysts contain the mesopores to accommodate the Ru nanoparticles, but their Ru content is not decreased by the subsequent coating. The Si/Al ratio (and the Al content of the catalyst) depends on the synthesis procedure. The parent ZSM-5, as well as the etched ZSM-5, has Si/Al = 21. The ZSM-5/Ru/ZSM-5 catalyst was prepared by coating with a sol having Si/Al ratio of 30 thus causing the decrease in the Si/Al ratio to Si/Al=27. Similarly, coating with pure silica sol

(giving S-1 shell) resulted in further increase to Si/Al=51. Coating of the initially pure silicalite-1 Ru/S-1 with Al containing sol (Si/Al=30) provided a catalyst with overall Si/Al=168. Note that these values represent an average over all the catalyst; the Si/Al ratio in the core part is preserved (that means Si/Al=21 and Si/Al=∞ for ZSM-5 and S-1 core, respectively).

Table 1: Composition, textural properties and concentration of acid sites in metal zeolite composite catalysts.

Catalyst Shell/Me/Core	**Ru[a], wt.%**	**Si/Al[b]**	**BET[c] m^2/g**	**V_{mic}[c], cm^3/g**	**V_{tot}[c], cm^3/g**	**S_{ext}, m^2/g**	**Brønsted sites[d], mmol/g**	**Lewis sites[d], mmol/g**
Ru/non etched S-1	5.9	∞	361	0.127	0.20	23	0	0
Ru/S-1	11.2	∞	371	0.131	0.20	21	0	0
Si/Ru/Si	5.2	∞	346	0.116	0.21	68	0	0
Ru/non-etched ZSM-5	8.4	21	375	0.130	0.19	22	0.487	0.042
Ru/ZSM-5	10.9	21	365	0.121	0.22	46	0.32	0.036
S-1/Ru/ZSM-5	5.9	51	320	0.104	0.23	49	0.168	0.03
ZSM-5/Ru/S-1	6.7	168	404	0.133	0.24	41	0.049	0.018
ZSM-5/Ru/ZSM-5	7.8	27	400	0.138	0.25	59	0.465	0.057

[a]Ru content was determined from integral H_2 consumption in a TPR experiment: [b] Si/Al ratio determined by ICP-OES;[c] Textural properties were determined from nitrogen sorption isotherms collected at -196°C; [d] concentration of acid sites was determined from pyridine adsorption/desorption at 150°C with FT-IR quantification of pyridinium species.

The acid sites are of the Brønsted character (approx. 90%), except for ZSM-5/Ru/S-1, where the share of Lewis acid sites reaches 27%. **Figure S5, SI** shows IR spectra used for calculation of the acid site concentration. In the spectra of silanol region after activation, the band at 3610 cm^{-1} evidences the presence of bridging Al-(OH)-Si groups (Brønsted acid sites). Only in the case of ZSM-5/Ru/S-1, its intensity is not sufficiently high to be visible. Nevertheless, the bands at 1545 cm^{-1} and 1455 cm^{-1}, observed after pyridine adsorption/desorption at 150°C, shows the presence of both Brønsted and Lewis acid sites, respectively, like in all other Al containing catalysts.

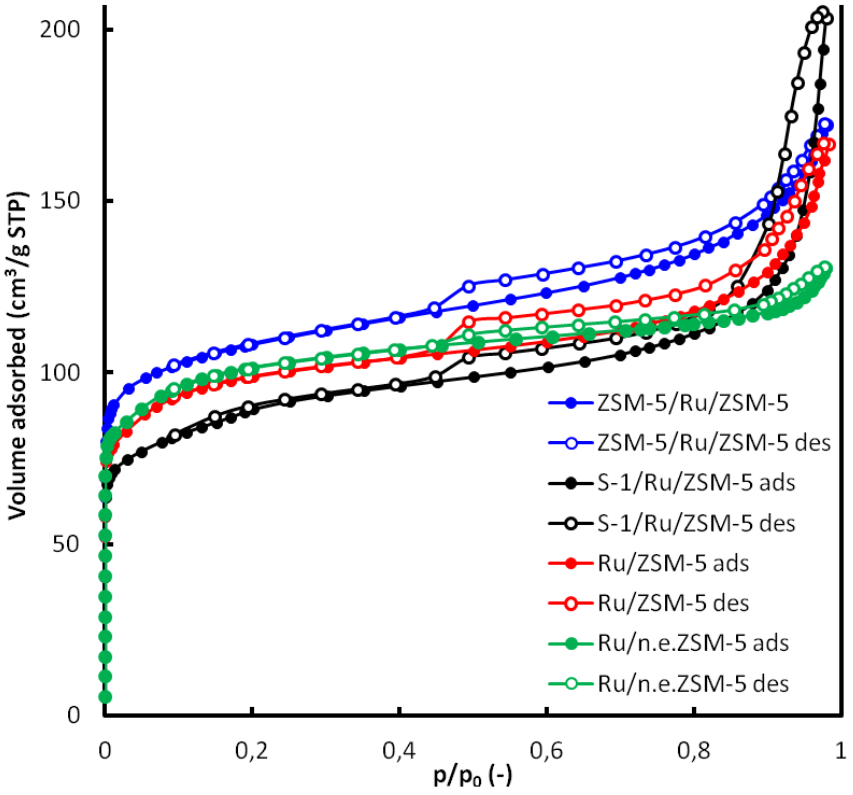

Figure 5: N_2 sorption isotherms of the catalysts with ZSM-5 core: ZSM-5/Ru/ZSM-5 (blue), S-1/Ru/ZSM-5 (black), Ru/ZSM-5 (red), Ru/n.e.ZSM-5 (green); empty points denote desorption.

Figures 5 and 6 present the nitrogen sorption isotherms, which served for the calculation of textural properties displayed in **Table 1**. The isotherm of Ru/non-etched ZSM-5 is very similar to the one of parent ZSM-5 before etching (not presented). The slight increase in the N_2 uptake at high p/p_0 results from interparticle adsorption in the agglomerates of Ru nanoparticles. Ru/ZSM-5 takes more N_2 into the etched mesopores at high p/p_0 (cf. TEM images). The coated ZSM-5/Ru/ZSM-5 and S-1/Ru/ZSM-5 show a hysteresis because of intercrystalline adsorption in the shell, which is composed of small ZSM-5 crystals. The high uptake above $p/p_0 = 0.9$ exhibited by S-1/Ru/ZSM-5 confirms that the shell is not 100% crystalline but there is no baseline elevation around $2\theta = 20° - 25°$ in the XRD pattern of this catalyst, which was observed for catalysts with completely amorphous shell (**Figure S3, SI**).

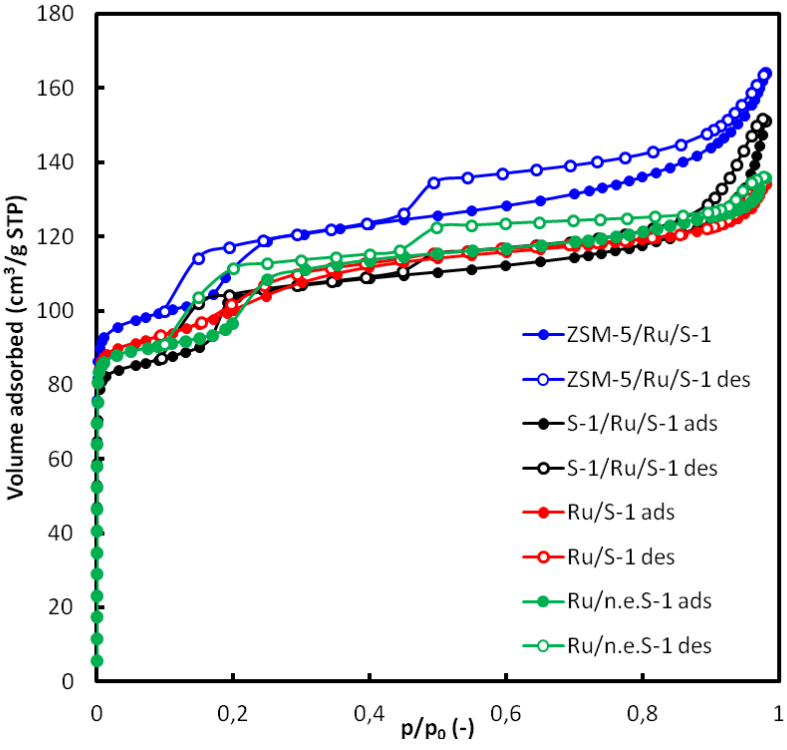

Figure 6: N_2 sorption isotherms of the catalysts with S-1 core: ZSM-5/Ru/S-1 (blue), S-1/Ru/S-1 (black), Ru/S-1 (red), Ru/n.e.S-1 (green); empty points denote desorption.

The catalysts prepared from S-1 parent exhibit an additional hysteresis at p/p_0 = 0.1 – 0.3 (**Figure 6**). The difference of the isotherm of S-1 based catalysts with the parent non-etched S-1 and etched S-1 (**Figure S6, SI**) is most probably due to the presence of Ru nanoparticles. This additional hysteresis (with another one at $p/p_0 = 10^{-4} – 10^{-2}$) has been observed before for high silica **MFI** zeolites [32,33] and it is not related to adsorption in mesopores (which occurs above relative pressure of 0.35). The origin of these hystereses is still under debate. So far, a possible explanation can be related to the occurrence of a phase transition between monoclinic and orthorhombic form of the **MFI** framework [34,35].

The shape of the hysteresis above p/p_0 = 0.45 for ZSM-5/Ru/S-1 together with the shape of the isotherm points to a well crystalline shell composed of small **MFI** crystals. For the Ru/S-1, the high relative pressure hysteresis is missing and in the Ru/non-etched S-1 it is significantly smaller resulting from interparticle adsorption in Ru agglomerates. The BJH pore size distribution curves are shown in **Figure S7, SI**. The BJH curves clearly illustrate the formation of mesopores upon fluoride etching and reconstruction of the material upon overgrowing. The presence of mesoporosity in S-1 crystallized on the surface of the parent crystals (S1-Ru-ZSM-5) also observed by SEM is possibly due to very fast crystallization so that the voids inside the crystals were not fully reconstructed. The peak at 3.7 nm present in the BJH curves of all samples is an artefact caused by breaking of meniscus of the liquid nitrogen at p/p_0 = 0.43.

In summary, the prepared Ru-**MFI** composite catalysts are composed of Ru nanoparticles of 3-20 nm (depending on preparation procedure), which are present on the surface of non-etched parent zeolite (Ru/non-etched S-1 and Ru/non-etchedZSM-5) or in the mesopores created by the ammonium fluoride etching (Ru/S-1 and Ru/ZSM-5). These zeolites can be covered by a layer,

which is composed of small secondary ZSM-5 or S-1 crystals formed during coating either with a ZSM-5 or a S-1 shell (four catalysts having a zeolite shell). The present set of catalysts enables to study the influence of the Ru location and influence of the acidic character of the parent (core) zeolite and coating shell on the catalytic performance in the hydrocarbon synthesis from syngas.

Table 2. Catalytic performance data of metal-zeolite composite catalysts. Conditions: GHSV=6500 cm^3/g.h, H_2/CO=2, P=20bar, T=250 °C

Catalyst Shell/Me/Core	**Ru wt. %**	**X_{CO}, %**	**R_{CO}, mol/g s**	**S_{CH4}, %**	**S_{C1-C12}, %**	**S_{C5-C12}, %**	**S_{C5+}, %**	**C_5-C_{12} iso/para ratio**
Ru/ non-etched S-1	5.9	9.0	7.25	4.2	36.8	22.7	85.9	1.6
Ru/S-1	11.2	29.5	23.79	12.0	51.7	29.9	78.2	1.8
Ru/non-etched ZSM-5	8.4	30.0	24.20	10.7	69.8	46.1	76.3	2.7
Ru/ZSM-5	10.9	49.1	39.60	12.1	88.8	62.2	73.4	3.2
S-1/Ru/S-1	4.7	8.0	6.45	10.0	47.6	26.6	79.0	1.9
Si-1/Ru/ZSM-5	5.9	23.2	18.71	12.4	61.5	36.8	75.3	1.9
ZSM-5/Ru/S-1	6.7	20.9	16.85	11.5	78.3	50.6	72.3	3.4
ZSM-5/Ru/ZSM-5	7.8	36.8	29.68	11.7	87.2	60.6	73.4	3.5

3.3.Catalytic performance in FT synthesis

The results of the FT catalytic evaluation of the materials are shown in **Table 2, Figure 7, Table S1 and Figures S8-S10, SI.** The reaction results in the production of hydrocarbons and water. Mostly C_1-C_{12} hydrocarbons were produced for metal-ZSM-5 catalysts. Only negligible amounts of carbon dioxide were detected. The dependence of carbon monoxide conversion over the studied catalysts as function of time on stream is displayed in **Figure S8, SI**. No visible deactivation was observed for all catalysts. This also suggests that no significant metal sintering or carbon deposition occur over the studied catalysts.

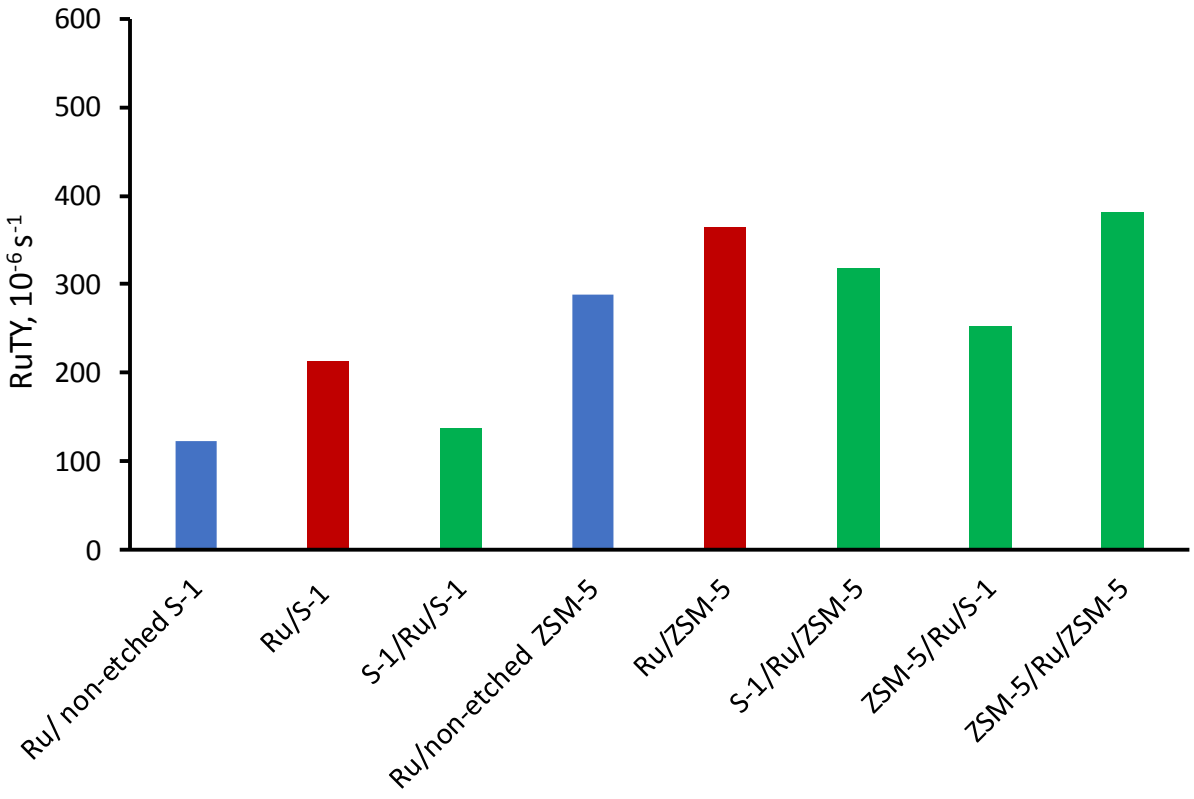

Figure 7: RuTY for ruthenium zeolite nanocomposite catalysts.

The catalytic performance is a function of ruthenium content in the samples; higher Ru content leads to high FT reaction rate (**Figure S9, SI**). Interestingly, the FT reaction rate does not correlate with the catalyst Brönsted acidity.The catalytic performance was also compared using ruthenium time-yield (RuTY), which was calculated as FT reaction rate normalized by the amount of Ru atoms in the catalyst. **Figure 7** shows that etching of either silicalite-1 or ZSM-5 results in a significant increase in the RuTY (e.g. S-1: 123.10^{-6} s^{-1} vs. 212.10^{-6} s^{-1}). Etching generates a complementary mesoporous structure in the zeolite support, where the Ru nanoparticles are subsequently deposited. Higher FT reaction rate over the etched catalysts can be, therefore, explained by the better dispersion of Ru nanoparticles over extrnal surface and mesopores of zeolite. Ru deposited on the etched support showed lower sintering ability during the catalyst calcination and reduction even in case, when it is not coated.

The selectivity of FT synthesis over Ru zeolite composite catalysts depends on both porosity, concentration and localization of acid sites within the catalyst. The Ru catalysts supported on S-1 (Ru/non-etched S-1, Ru/S-1, S-1/Ru/S-1) showed the highest selectivity to the C_{5+} hydrocarbons (85.9%, 78.2% and 79%, respectively) and lowest ratio of iso- to normal hydrocarbons among all the studied samples (1.6, 1.8, 1.9, respectively, **Table 2**). At the same time, the silicalite-1 etching and coating of the etched sample with a silicalite-1 layer (S-1/Ru/S-1) result in higher selectivity to methane and lighter hydrocarbons, some decrease in the C_{5+} selectivity and higher CO conversion in comparison with Ru/non etched S-1. The effect can be again due to the localization of smaller Ru nanoparticles within the zeolite mesopores in Ru/S-1. In addition, the S-1/Ru/S-1 provided lower CO conversion in comparison with Ru/S-1 not only becase of lower Ru content (Ru/S-1 11.2 wt.% vs. S-1/Ru/S-1 4.7 wt.% = ratio 2.4:1) but also because of creating additional diffusional limitation due the catalyst coating with silicalite-1 layer in the S-1/Ru/S-1

sample (CO conversion 29.6% vs. 8% = ratio 3.7:1). These results are consistent with previous reports [8,36,37]. The hydrocarbon distribution curves for coated S-1/Ru/S1, S-1/Ru/ZSM-5, ZSM/Ru/S-1 and ZSM-5/Ru/ZSM-5 catalyst are displayed in **Figure S10, SI**. They also clearly show high fraction of iso-paraffins in the catalysts containing ZSM-5 in the shell (ZSM-5/Ru/S-1 and ZSM-5/Ru/ZSM-5).

The Ru catalysts supported on both non-etched and etched ZSM-5 zeolite exhibit higher selectivity to shorter hydrocarbons in comparison with their S-1 based counterparts (e.g. S_{C5-C12} over Ru/S-1 29.9% vs. Ru/ZSM-5 62.2%) and at the same time higher ratio of iso- to normal hydrocarbons in the C_5-C_{12} hydrocarbons range is observed for these pairs (e.g. Ru/S-1 1.8 *vs.* Ru/ZSM-5 3.2, **Table 2**). The observed phenomena are due to the isomerization and cracking of the hydrocarbons, produced during FT synthesis, over the ZSM-5 zeolite acid sites.

Interesting results are observed for the Ru-zeolite catalysts coated with a layer of silicalite-1 or ZSM-5 zeolite. Coating of ZSM-5 zeolites containing Ru nanoparticles with silicalite-1 (S-1/Ru/ZSM-5) results in the selectivity patterns similar to that observed over the silicalite-1 based samples such as Ru/S-1, Ru/non-etched S-1 or S-1/Ru/S-1 catalysts. This suggests that the presence of the silicalite-1 shell on the top of any of the Ru zeolite catalysts significantly reduces the isomerization activity. Coating with silicalite results in the decrease in the concentration of the Brønsted acid sites in the proximity to Ru nanoparticles and thus, results in lower selectivity to iso-paraffins.

Somewhat different results were obtained over the catalysts containing the shell constituted by the ZSM-5 zeolite (regardless the core). Both ZSM-5/Ru/ZSM-5 and ZSM-5/Ru/S-1 catalysts exhibited rather similar selectivity to methane (S_{CH4} = 11.5 %), to C_5 and longer hydrocarbons (S_{C5+} = 72.3 %) and iso/n ratio (3.4) and, together with Ru/ZSM-5 without shell, they provided

the highest selectivity for the gasoline hydrocarbons of all the investigated catalysts (S_{C5-12} 60.6%, 50.6% and 62.2%, respectively). Thus, the catalysts which contain the ZSM-5 zeolite in the shell, showed the highest isomerization activity and respectively highest ratio of the iso- to normal hydrocarbons. This is indicative of the important and probably determining role of the acid sites located in the shell on the selectivity patterns.

The catalytic data were also measured at higher temperature (270°C, **Table S1, SI**). They show slightly lower selectivity to C_{5+} hydrocarbons and further increase in the ratio of iso- to normal paraffins over the catalysts containing the acid ZSM-5 zeolite in the catalyst shell.

3.4.Roles of core, shell and porosity in the Ru-zeolite nanocomposite catalysts in the synthesis of iso-paraffins from syngas

Our results indicate that the zeolite mesoporosity has an essential influence on the performance of ruthenium zeolite composite catalysts. The most noticeable effect is higher FT reaction rate observed at the same Ru content over the mesoporous samples (**Figure 7**). In agreement with previous reports [13,18], the presence of mesopores facilitates diffusion of carbon monoxide and hydrocarbons within the catalyst pellets. The presence of mesopores reduces the effective H_2/CO ratio in the proximity to the active sites and lowers methane selectivity. Note that synthesis of iso-paraffins from syngas over Ru zeolite composite catalysts involves both metal and acid sites. First, the metal sites are required for CO hydrogenation to hydrocarbons via FT reaction. FT reaction involves adsorption and dissociation of carbon monoxide and hydrogen on the metal sites followed by surface polymerization of adsorbed CH_x fragments, their hydrogenation, and desorption [1,18]. FT synthesis results in the production of mostly linear hydrocarbons. Formation

of iso-paraffins under FT reaction conditions demands hydrocarbon isomerization. Isomerization of paraffins on zeolite in the absence of metals requires high temperatures and often coincides with major cracking. It is not likely, therefore, that paraffin isomerization solely catalyzed by zeolite acid sites may occur under the conditions of FT synthesis. Taking into account the temperatures typically used for low temperature FT synthesis (190-240°C), the hydrocarbon isomerization under these conditions should also involve metal sites. Thus, the role of ruthenium metal sites could also be related to dehydrogenation of FT hydrocarbons providing olefins for isomerization. In this case, olefin isomerization occur on the acid sites associated with the zeolite. Both paraffins and olefins are primary products of FT synthesis over Ru catalysts. While olefin isomerization does not require metal sites, paraffin isomerization takes place on both metal and acid sites. It can be favored therefore by their proximity.

The catalysts in this paper were prepared by insertion of Ru nanoparticles on and into ZSM-5 or silicalite-1 zeolites. The inserted nanoparticles are preferentially located on the outer surface of the zeolite particles. Generation of additional mesoporosity by etching results in partial encapsulation of these nanoparticles and their localization in the mesopores in the subsurface layer of the zeolite. Subsequent coating (overgrowing) introduces the silicalite-1 or ZSM-5 zeolite shell in direct interaction with Ru nanoparticles. Our characterization results are indicative of the stability of Ru/ZSM-5 and Ru/S-1 during the coating process. Indeed, the textural properties of the zeolite (apparent surface area, microporous volume) are only slightly affected by the coating (**Table 1**, **Figures 5** and **6**). The XRD patterns of ZSM-5 and S-1 remain unchanged after the coating (see **Figure 2**).

The catalytic results suggest that in the coated samples, ruthenium nanoparticles interact more strongly with the coating materials (silicalite-1 or ZSM-5) than with the catalyst core. In

addition, any formed hydrocarbons are forced to pass through the layer of zeolite phase, where they undergo isomerization/cracking. This explains the observed determining effect of the catalyst shell on the reaction selectivity. The isomerization activity of the catalyst is much more significantly affected by the shell of the composite catalysts than by the core. The isomerization of olefins takes place mostly in the very close proximity of the ruthenium nanoparticles, which are preferentially localized on the outer surface of the core crystals, or in the sub-surface layer (in the case of etched samples).

Our results suggest that the presence of Brønsted acid sites in the close proximity to ruthenium nanoparticles is indispensable in order to attain higher ratio of olefin to pararffins. Higher concentration of Brønsted acid sites in the proximity of ruthenium nanoparticles can be attained by creating core-shell structure with the shell formed by ZSM-5 zeolite. The presence of Brønsted acid sites in this shell is extremely important for higher selectivity to iso-paraffins. This shell is even more important than the catalyst core. For example, the catalysts, which are composed by silica core (without acid sites) and zeolite shell formed by ZSM-5 zeolite, have shown good performance in synthesis of iso-paraffins from syngas. The conclusion about inference of the shell and its acidity on the reaction selectivity has a fundamental significance for the design of bifunctional catalysts.

4. Conclusion

Ruthenium-zeolite composite catalysts for FT reaction have been prepared and studied with the aim to encapsulate the metallic nanoparticles inside the zeolite matrix to provide high “intimacy” between the metallic and acid active sites of the catalyst.

Efficient encapsulation of ruthenium nanoparticles within the zeolite crystals was successfully achieved by coating the ZSM-5 and silicalite-1 carriers containing Ru nanoparticles with a shell MFI-type material. The synthesis procedure involves thee steps: (i) creation of mesopores in the parent zeolite by etching with ammonium fluoride, (ii) synthesis of ruthenium nanoparticles and their deposition over parent non-etched or etched zeolites, (iii) zeolite overgrowing (coating) of the Ru-zeolite catalysts. In these composite materials, ruthenium nanoparticles are covered a thin layer of a zeolite shell.

The catalytic performance of the synthesized materials primarily depends on the ruthenium content, the presence of secondary mesopores and the composition and acidity of the catalyst shell. The reaction rates increase with higher Ru content. The diffusion limitations in the composite catalysts are reduced by using mesoporous ZSM-5 or silicalite-1 as core. Significantly increased relative amount of produced iso-paraffins (with respect to n-paraffins) was observed over the catalysts containing the ZSM-5 zeolite in the shell. Isomerization of hydrocarbons produced via FT synthesis requires the presence of both metal and acid sites. The proximity between these sites in the zeolite shell is a crucial parameter for the design of efficient metal zeolite bifunctional catalysts for selective synthesis of gasoline type fuels via FT synthesis. The acidity of the catalyst core has only a limited impact on the catalytic performance.

Supporting Information

Catalytic performance measured at 270 °C; powder XRD patterns; histogram of ruthenium particle size distribution; IR spectra of the metal-zeolite catalysts; N_2 sorption isotherms; BJH pore size distribution curves; carbon monoxide conversion as a function of time on stream; FT reaction rate versus Ru content; hydrocarbon distribution graphs

Acknowledgements

The authors are grateful to Olivier Gardoll, Laurence Burylo and Joelle Thuriot for help with TPR, XRD and XRF measurements. The authors acknowledge the financial support of the French National Research Agency (DirectSynBioFuel project, Ref. ANR-15-CE06-0004 and NANO4-FUT, Ref. ANR-16-CE06-0013). Chevreul Institute (FR 2638), Ministère de l'Enseignement Supérieur, de la Recherche et de l'Innovation, Hauts-de-France Region and FEDER are acknowledged for supporting and funding partially this work.

Reference

(1) Khodakov, A. Y.; Chu, W.; Fongarland, P. Advances in the Development of Novel Cobalt Fischer-Tropsch Catalysts for Synthesis of Long-Chain Hydrocarbons and Clean Fuels. *Chem. Rev.* **2007**, *107*, 1692–1744.

(2) Zhou, W.; Cheng, K.; Kang, J.; Zhou, C.; Subramanian, V.; Zhang, Q.; Wang, Y. New Horizon in C1 Chemistry: Breaking the Selectivity Limitation in Transformation of Syngas and Hydrogenation of CO_2 into Hydrocarbon Chemicals and Fuels. *Chem. Soc. Rev.* **2019**, *48*, 3193–3228.

(3) Komvokis, V. G.; Karakoulia, S.; Iliopoulou, E. F.; Papapetrou, M. C.; Vasalos, I. A.; Lappas, A. A.; Triantafyllidis, K. S. Upgrading of Fischer–Tropsch Synthesis Bio-Waxes via Catalytic Cracking: Effect of Acidity, Porosity and Metal Modification of Zeolitic and Mesoporous Aluminosilicate Catalysts. *Catal. Today* **2012**, *196*, 42–55.

(4) Li, J.; He, Y.; Tan, L.; Zhang, P.; Peng, X.; Oruganti, A.; Yang, G.; Abe, H.; Wang, Y.; Tsubaki, N. Integrated Tuneable Synthesis of Liquid Fuels via Fischer–Tropsch Technology. *Nat. Catal.* **2018**, *1*, 787–793.

(5) Zhang, Q.; Kang, J.; Wang, Y. Development of Novel Catalysts for Fischer-Tropsch Synthesis: Tuning the Product Selectivity. *ChemCatChem* **2010**, *2*, 1030–1058.

(6) Weisz, P. B. Polyfunctional Heterogeneous Catalysis. *Adv. Catal.* **1962**, *13*, 137–190.

(7) Martínez, A.; Valencia, S.; Murciano, R.; Cerqueira, H. S.; Costa, A. F.; S.-Aguiar, E. F. Catalytic Behavior of Hybrid Co/SiO_2-(Medium-Pore) Zeolite Catalysts during the One-Stage Conversion of Syngas to Gasoline. *Appl. Catal. A Gen.* **2008**, *346*, 117–125.

(8) Cheng, K.; Kang, J.; Huang, S.; You, Z.; Zhang, Q.; Ding, J.; Hua, W.; Lou, Y.; Deng,

W.; Wang, Y. Mesoporous Beta Zeolite-Supported Ruthenium Nanoparticles for Selective Conversion of Synthesis Gas to C_5–C_{11} Isoparaffins. *ACS Catal.* **2012**, *2*, 441–449.

(9) Sartipi, S.; Makkee, M.; Kapteijn, F.; Gascon, J. Catalysis Engineering of Bifunctional Solids for the One-Step Synthesis of Liquid Fuels from Syngas: A Review. *Catal. Sci. Technol.* **2014**, *4*, 893–907.

(10) Sartipi, S.; Van Dijk, J. E.; Gascon, J.; Kapteijn, F. Toward Bifunctional Catalysts for the Direct Conversion of Syngas to Gasoline Range Hydrocarbons: H-ZSM-5 Coated Co versus H-ZSM-5 Supported Co. *Appl. Catal. A Gen.* **2013**, *456*, 11–22.

(11) Martínez-Vargas, D. X.; Sandoval-Rangel, L.; Campuzano-Calderon, O.; Romero-Flores, M.; Lozano, F. J.; Nigam, K. D. P.; Mendoza, A.; Montesinos-Castellanos, A. Recent Advances in Bifunctional Catalysts for the Fischer–Tropsch Process: One-Stage Production of Liquid Hydrocarbons from Syngas. *Ind. Eng. Chem. Res.* **2019**, *58*, 15872–15901.

(12) Flores, C.; Batalha, N.; Marcilio, N. R.; Ordomsky, V. V.; Khodakov, A. Y. Influence of Impregnation and Ion Exchange Sequence on Metal Localization, Acidity and Catalytic Performance of Cobalt BEA Zeolite Catalysts in Fischer-Tropsch Synthesis. *ChemCatChem* **2019**, *11*, 568–574.

(13) Kim, J.-C.; Lee, S.; Cho, K.; Na, K.; Lee, C.; Ryoo, R. Mesoporous MFI Zeolite Nanosponge Supporting Cobalt Nanoparticles as a Fischer–Tropsch Catalyst with High Yield of Branched Hydrocarbons in the Gasoline Range. *ACS Catal.* **2014**, *4* , 3919–3927.

(14) Fraenkel, D.; Gates, B. C. Shape-Selective Fischer-Tropsch Synthesis Catalyzed by Zeolite-Entrapped Cobalt Clusters. *J. Am. Chem. Soc.* **1980**, *102*, 2478–2480.

(15) Bao, J.; He, J.; Zhang, Y.; Yoneyama, Y.; Tsubaki, N. A Core/Shell Catalyst Produces a

Spatially Confined Effect and Shape Selectivity in a Consecutive Reaction. *Angew. Chemie Int. Ed.* **2008**, *47*, 353–356.

(16) Subramanian, V.; Zholobenko, V. L.; Cheng, K.; Lancelot, C.; Heyte, S.; Thuriot, J.; Paul, S.; Ordomsky, V. V.; Khodakov, A. Y. The Role of Steric Effects and Acidity in the Direct Synthesis of Iso-Paraffins from Syngas on Cobalt Zeolite Catalysts. *ChemCatChem* **2016**, *8*, 380–389.

(17) Carvalho, A.; Marinova, M.; Batalha, N.; Marcilio, N. R.; Khodakov, A. Y.; Ordomsky, V. V. Design of Nanocomposites with Cobalt Encapsulated in the Zeolite Micropores for Selective Synthesis of Isoparaffins in Fischer-Tropsch Reaction. *Catal. Sci. Technol.* **2017**, *7*, 5019–5027.

(18) Iglesia, E.; Reyes, S. C.; Madon, R. J.; Soled, S. L. Selectivity Control and Catalyst Design in the Fischer-Tropsch Synthesis: Sites, Pellets, and Reactors. *Adv. Catal.* **1993**, *39*, 221–302.

(19) He, J.; Liu, Z.; Yoneyama, Y.; Nishiyama, N.; Tsubaki, N. Multiple-Functional Capsule Catalysts: A Tailor-Made Confined Reaction Environment for the Direct Synthesis of Middle Isoparaffins from Syngas. *Chem. - A Eur. J.* **2006**, *12*, 8296–8304.

(20) He, J.; Yoneyama, Y.; Xu, B.; Nishiyama, N.; Tsubaki, N. Designing a Capsule Catalyst and Its Application for Direct Synthesis of Middle Isoparaffins. *Langmuir* **2005**, *21*, 1699–1702.

(21) Zhu, C.; Bollas, G. M. Gasoline Selective Fischer-Tropsch Synthesis in Structured Bifunctional Catalysts. *Appl. Catal. B Environ.* **2018**, *235*, 92–102.

(22) Liu, J.-Y.; Chen, J.-F.; Zhang, Y. Cobalt-Imbedded Zeolite Catalyst for Direct Syntheses of Gasoline via Fischer–Tropsch Synthesis. *Catal. Sci. Technol.* **2013**, *3*, 2559-2564.

(23) Mazonde, B.; Cheng, S.; Zhang, G.; Javed, M.; Gao, W.; Zhang, Y.; Tao, M.; Lu, C.; Xing, C. A Solvent-Free: In Situ Synthesis of a Hierarchical Co-Based Zeolite Catalyst and Its Application to Tuning Fischer-Tropsch Product Selectivity. *Catal. Sci. Technol.* **2018**, *8*, 2802–2808.

(24) Liu, J.; Wang, D.; Chen, J.-F.; Zhang, Y. Cobalt Nanoparticles Imbedded into Zeolite Crystals: A Tailor-Made Catalyst for One-Step Synthesis of Gasoline from Syngas. *Int. J. Hydrogen Energy* **2016**, *41*, 21965–21978.

(25) Cheng, S.; Mazonde, B.; Zhang, G.; Javed, M.; Dai, P.; Cao, Y.; Tu, S.; Wu, J.; Lu, C.; Xing, C.; et al. Co-Based MOR/ZSM-5 Composite Zeolites over a Solvent-Free Synthesis Strategy for Improving Gasoline Selectivity. *Fuel* **2018**, *223*, 354–359.

(26) Flores, C.; Batalha, N.; Ordomsky, V. V.; Zholobenko, V. L.; Baaziz, W.; Marcilio, N. R.; Khodakov, A. Y. Direct Production of Iso-Paraffins from Syngas over Hierarchical Cobalt-ZSM-5 Nanocomposites Synthetized by Using Carbon Nanotubes as Sacrificial Templates. *ChemCatChem* **2018**, ***10***, 2291-2299.

(27) Flores, C.; Zholobenko, V. L.; Gu, B.; Batalha, N.; Valtchev, V.; Baaziz, W.; Ersen, O.; Marcilio, N. R.; Ordomsky, V. V.; Khodakov, A. Y. Versatile Roles of Metal Species in Carbon Nanotube Templates for the Synthesis of Metal–Zeolite Nanocomposite Catalysts. *ACS Appl. Nano Mater.* **2019**, *2*, 4507–4517.

(28) Qin, Z.; Melinte, G.; Gilson, J.-P.; Jaber, M.; Bozhilov, K.; Boullay, P.; Mintova, S.; Ersen, O.; Valtchev, V. The Mosaic Structure of Zeolite Crystals. *Angew. Chemie* **2016**, *128*, 15273–15276.

(29) Subramanian, V.; Cheng, K.; Lancelot, C.; Heyte, S.; Paul, S.; Moldovan, S.; Ersen, O.; Marinova, M.; Ordomsky, V. V.; Khodakov, A. Y. Nanoreactors: An Efficient Tool to

Control the Chain-Length Distribution in Fischer-Tropsch Synthesis. *ACS Catal.* **2016**, *6*, 1785-1792.

(30) Lippens, B. Studies on Pore Systems in Catalysts V. The t Method. *J. Catal.* **1965**, *4*, 319–323.

(31) Ngoye, F.; Lakiss, L.; Qin, Z.; Laforge, S.; Canaff, C.; Tarighi, M.; Valtchev, V.; Thomas, K.; Vicente, A.; Gilson, J. P.; et al. Mitigating Coking during Methylcyclohexane Transformation on HZSM-5 Zeolites with Additional Porosity. *J. Catal.* **2014**, *320*, 118–126.

(32) Müller, U.; Unger, K. K. Sorption Studies on Large ZSM-5 Crystals: The Influence of Aluminium Content, The Type of Exchangeable Cations and the Temperature on Nitrogen Hysteresis Effects. *Stud. Surf. Sci. Catal.* **1988**, *39*, 101-108.

(33) Nakai, K.; Sonoda, J.; Yoshida, M.; Hakuman, M.; Naono, H. High Resolution Adsorption Isotherms of N_2 and Ar for Nonporous Silicas and MFI Zeolites. *Adsorption* **2007**, *13*, 351–356.

(34) Parra, J. B.; Ania, C. O.; Dubbeldam, D.; Vlugt, T. J. H.; Castillo, J. M.; Merkling, P. J.; Calero, S. Unraveling the Argon Adsorption Processes in MFI-Type Zeolite. *J. Phys. Chem. C* **2008**, *112*, 9976–9979.

(35) Cychosz, K. A.; Guillet-Nicolas, R.; García-Martínez, J.; Thommes, M. Recent Advances in the Textural Characterization of Hierarchically Structured Nanoporous Materials. *Chem. Soc. Rev.* **2017**, *46*, 389–414.

(36) Kang, J.; Cheng, K.; Zhang, L.; Zhang, Q.; Ding, J.; Hua, W.; Lou, Y.; Zhai, Q.; Wang, Y. Mesoporous Zeolite-Supported Ruthenium Nanoparticles as Highly Selective Fischer-Tropsch Catalysts for the Production of C_5-C_{11} Isoparaffins. *Angew. Chemie - Int. Ed.*

2011, *50*, 5200–5203.

(37) Zhang, Q.; Cheng, K.; Kang, J.; Deng, W.; Wang, Y. Fischer-Tropsch Catalysts for the Production of Hydrocarbon Fuels with High Selectivity. *ChemSusChem* **2014**, *7*, 1251–1264.